Hindawi Publishing Corporation
Advances in Meteorology
Volume 2016, Article ID 4126393, 11 pages
http://dx.doi.org/10.1155/2016/4126393

Research Article

An Algorithm for Retrieving Precipitable Water Vapor over Land Based on Passive Microwave Satellite Data

Fang-Cheng Zhou,[1,2] Xiaoning Song,[2] Pei Leng,[3] Hua Wu,[1,4] and Bo-Hui Tang[1,4]

[1] *State Key Laboratory of Resources and Environment Information System, Institute of Geographic Sciences and Natural Resources Research, Chinese Academy of Sciences, Beijing 100101, China*
[2] *University of Chinese Academy of Sciences, Beijing 100049, China*
[3] *Key Laboratory of Agri-Informatics, Ministry of Agriculture/Institute of Agricultural Resources and Regional Planning, Chinese Academy of Agricultural Sciences, Beijing 100081, China*
[4] *Jiangsu Center for Collaborative Innovation in Geographical Information Resource Development and Application, Nanjing 210023, China*

Correspondence should be addressed to Xiaoning Song; songxn@ucas.ac.cn

Received 20 October 2015; Revised 5 January 2016; Accepted 11 January 2016

Academic Editor: James Cleverly

Precipitable water vapor (PWV) is one of the most variable components of the atmosphere in both space and time. In this study, a passive microwave-based retrieval algorithm for PWV over land without land surface temperature (LST) data was developed. To build the algorithm, two assumptions exist: (1) land surface emissivities (LSE) at two adjacent frequencies are equal and (2) there are simple parameterizations that relate transmittance, atmospheric effective radiating temperature, and PWV. Error analyses were performed using radiosonde sounding observations from Zhangye, China, and CE318 measurements of Dalanzadgad (43°34′37″N, 104°25′8″E) and Singapore (1°17′52″N, 103°46′48″E) sites from Aerosol Robotic Network (AERONET), respectively. In Zhangye, the algorithm had a Root Mean Square Error (RMSE) of 4.39 mm and a bias of 0.36 mm on cloud-free days, while on cloudy days there was an RMSE of 4.84 mm and a bias of 0.52 mm because of the effect of liquid water in clouds. The validations in Dalanzadgad and Singapore sites showed that the retrieval algorithm had an RMSE of 4.73 mm and a bias of 0.84 mm and the bigger errors appeared when the water vapor was very dry or very moist.

1. Introduction

Precipitable water vapor (PWV) is an important atmospheric component that influences many atmospheric processes [1]. It is also crucial for studies of climate change and global warming because water vapor is the most abundant greenhouse gas [2]. In the field of quantitative remote sensing, knowledge of PWV can help improve the retrieval accuracy for many parameters because of the atmospheric correction to remote sensing images [3–6].

A number of methods have been developed to estimate PWV, either from ground surveys or from remote sensing [7]. Instrumental measurements of PWV are generally made with radiosondes, ground-based Global Positioning Systems (GPS), microwave radiometers, sun photometers, Raman lidar systems, Fourier-Transform spectrometers, and space-based satellites with near-infrared or thermal-infrared spectrometers or microwave sounders [8–25]. In particular, radiosonde PWV were the standard PWV for many decades [11]. However, the use of radiosondes is restricted by their high operational cost and poor spatial resolution. Sun photometers operating in the strong water vapor absorption band have been used to determine PWV, but they are limited to be clear of clouds on the path to the Sun [13–16]. The main advantage of Raman lidar approach is that the laser source does not have to turn a specific water vapor absorption line [17–21]. Dual-frequency, ground-based microwave radiometers have been used for more than 30 years to derive both PWV and cloud liquid water; they use frequency bands around the water vapor absorption line at 22.235 GHz.

Ground-based microwave radiometers can operate in a continuous and unattended manner under almost all weather conditions with high temporal resolution and low uncertainty [22–25]. Ground-based GPS is an increasingly useful tool for measuring PWV, agreeing with radiosonde data within 1-2 mm [26–28]. However, ground-based microwave radiometers and GPS methods cannot assess the distribution of PWV on a global scale, a problem that also affects ground surveys because of their poor coverage over oceans and lakes. Thus, in comparison with these ground-based measurements, space-based surveys are an effective way to obtain global PWV data. Many algorithms have been developed to estimate PWV from satellite data. For example, MODIS includes two PWV products derived from observations in the near-infrared and thermal-infrared channels [29]. However, Li et al. [30] found that MODIS algorithms overestimated PWV compared to data from radiosondes and ground-based GPS. Moreover, because the MODIS PWV products are based on measurements from the near-infrared or thermal-infrared channels, they perform poorly in cloudy conditions. Jet Propulsion Laboratory (JPL) Atmospheric Infrared Sounder (AIRS) is the first of a new generation of advanced satellite-based atmospheric sounders with the capability of obtaining high-vertical resolution profiles of temperature and water vapor [31, 32]. Although it can produce moisture profile under partial cloud cover, the spatial resolutions of PWV products are sparse [33].

Compared with infrared measurements, space-based passive microwave observations have the advantage of being able to detect PWV on both cloud-free and cloudy days because microwaves can penetrate clouds. However, the use of passive microwave satellite data for PWV estimation has traditionally been applied only over oceans because of their relatively simple surface conditions compared to the land surface. In general, two methods are used to estimate PWV over oceans. The first uses physical algorithms that employ radiative transfer theory in the model derivations (e.g., the multiple linear regression algorithms developed by Schluessel and Emery [34] and the nonlinear iterative algorithms developed by Wentz and Meissner [35]). The second method involves purely statistical methods with little or no consideration of the underlying physics (e.g., the postlaunch *in situ* regression algorithms of Basili et al. [36]). Compared to oceans, development of PWV retrieval algorithms over land surfaces has been slow because these surfaces have high pixel-to-pixel variability in their surface emissivity, which makes it difficult to distinguish the atmospheric signal from the surface background [37]. Nevertheless, several recent approaches have been proposed that ignore the sensitivity of PWV to land surface emissivity (LSE). Some use a neural network approach with a database acquired from the radiative transfer model [38–40], and some take advantage of high frequency water vapor channels, such as 150.00 and around 183.31 GHz, which show very low sensitivity to the change in LSE during PWV estimation [41, 42]. While these two methods are feasible, both have disadvantages: the former has a limited physical basis and the latter cannot be used for datasets that do not include high frequency water vapor channels, such as those from the Special Sensor Microwave Imager (SSM/I), the Scanning Multichannel Microwave Radiometer (SMMR), and the Advanced Microwave Scanning Radiometer-Earth Observing System (AMSR-E). Although Deeter [43] proposed an algorithm for PWV estimation over both land and ocean based on brightness temperatures at 18.7 and 23.8 GHz, the algorithm did not explain why these two frequencies were selected [44]. Based on these deficiencies, the objective of this study is to develop an algorithm for retrieving PWV over land using passive microwave satellite data at low frequencies.

The paper is organized as follows: Section 2 describes the data used in this study; Section 3 describes the retrieval algorithm from a semiempirical point of view; Section 4 explains the sensitivity analysis and validation with independent datasets; and Section 5 concludes the paper.

2. Data

2.1. The Thermodynamic Initial Guess Retrieval (TIGR) Dataset. The TIGR dataset was constructed by the Laboratoire de Meteorologie Dynamique and includes 2311 atmospheric profiles selected from 80,000 radiosonde datasets. These profile data are located around the world and represent real atmosphere conditions. Each atmospheric profile records temperature, water vapor, and ozone concentrations on a given pressure grid from the surface to the top of the atmosphere.

In this study, 378 cloud-free and overland atmospheric profiles located between 30 and 60 degrees north from the TIGR dataset were downloaded from the Atmospheric Radiation Analysis (ARA) website [46]. Using these profiles, we built a dataset including transmittances, atmospheric effective radiating temperatures, and PWV to develop the PWV retrieval model.

2.2. Microwave Radiation Imager (MWRI) Data. Launched on 5 November 2010, FengYun-3B (FY-3B) is the second satellite in the Chinese FY satellite series. FY-3B crosses the equator in the ascending mode at 13:40 h local solar time. The Microwave Radiation Imager (MWRI) on board FY-3B is a passive microwave imager that uses conical scanning at an incidence angle of 53°. It is a total-power passive radiometer that measures radiation at five frequencies (10.65, 18.7, 23.8, 36.5, and 89.0 GHz) with vertical and horizontal polarization [45]. A detailed description of the characteristics of the FY-3B MWRI is provided in Table 1.

In this study, brightness temperatures derived from the FY-3B MWRI with a unified resolution of 10 km were acquired from the National Satellite Meteorological Centre [47] and used to provide input parameters for the PWV retrieval algorithm.

2.3. Radiosonde Sounding Observations. Located in Zhangye City, Gansu Province, China, the Zhangye National Climate Observatory (39°5′15.68″N, 100°16′39.11″E) was selected as the validation area for this study. The estimated PWV was verified using PWV data from the observatory's sounding observations.

Table 1: Performance requirements for the FY-3B MWRI [45].

Frequencies (GHz)	10.65	18.7	23.8	36.5	89
Polarization	V/H	V/H	V/H	V/H	V/H
Bandwidth (MHz)	180	200	400	400	3000
Sensitivity (K)	0.5	0.5	0.5	0.5	0.8
Calibration error (K)	1.5	1.5	1.5	1.5	1.5
Dynamic range (K)	3–340				
Samples/scan	254				
Main beam efficiency	>90%				
Ground resolution (km)	51 × 85	30 × 50	27 × 45	18 × 30	9 × 15
Scan mode	Conical scanning				
Orbit width (km)	1400				
Viewing angle (deg)	45				
Scan period (s)	1.8				

At Zhangye National Climate Observatory, L band Vaisala RS92 radiosonde balloons were launched three times per day, at 7:00–8:00 h, 13:00–14:00 h, and 19:00–20:00 h local solar time, from June 1, 2012, to August 31, 2012. In this study, we used the observations from 13:00 to 14:00 h because they corresponded to the transit time of FY-3B. The L band radiosonde system [48] records pressure, temperature, relative humidity, wind speed, and wind direction profiles. The radiosonde balloons ascend to approximately 30–35 km in the sky; namely, they record atmospheric information from the land surface to 30 km above the ground.

Vaisala radiosondes use thin-film capacitance relative humidity sensors. The capacitance measured by the radiosonde is proportional to the number of water molecules captured at binding sites in the polymer, structure, which in turn is proportional to the ambient water vapor concentration. Miloshevich et al. [49] found that RS92 mean bias for daytime soundings and high solar altitude angles was a dry bias that increases from about 5% at 700 mbar to 45% in the upper troposphere and varies somewhat with relative humidity. The radiosonde PWV would be used as the true values to validate the retrieval algorithm; consequently, the mean bias error of Vaisala RS92 measurements was firstly removed by an empirical correction [49] in this study.

2.4. Aerosol Robotic Network (AERONET) Sun Photometers. Aerosol Robotic Network (AERONET) [50] makes measurements of the Sun direct irradiance and performs PWV retrievals based on CE318 sun photometers measurements in the water vapor absorption band around 940 nm. AERONET was created basically for studying columnar aerosol properties, and the quality of those retrievals was well established [50–52]. Two sites located at Dalanzadgad (43°34′37″N, 104°25′8″E, in dry area) and Singapore (1°17′52″N, 103°46′48″E, in tropical region) operated by AERONET were chosen as other validation areas. The validation time was still from June 1, 2012, to August 31, 2012, at around 05:40 h Greenwich Mean Time (GMT).

In general, even Level 2.0 (best data quality offered by AERONET) PWV products were lower than those obtained by ground-based microwave radiometers and GPS by ~6.0–9.0% and ~6.0–8.0%, respectively. The AERONET values were also lower by approximately 5% than those obtained from the balloon radiosondes [12]. Consequently, the PWV from AERONET need to be corrected based on [12] firstly and then to be used to validate the retrieval PWV.

3. Methodology

3.1. Model Development. The brightness temperature T_B measured using space-based microwave radiometers consists of three radiative components: (1) the upwelling radiation emitted by the atmosphere, $T_a^{\uparrow}$; (2) the radiation emitted from the surface that is attenuated by the atmosphere, $\tau \cdot \varepsilon \cdot T_s$; and (3) the downwelling radiation from the atmosphere and the cosmic background that is reflected by the surface and attenuated by the atmosphere, $(1-\varepsilon)\tau(T_a^{\downarrow} + T_{\text{sky}})$. Assuming that the land surface is Lambertian and that the upwelling and downwelling atmospheric radiances are identical [53], the radiative transfer equations at two frequencies can be written as follows:

$$T_{B,i} = T_{a,i} + \tau_i \cdot \varepsilon_i \cdot T_s + \left(1-\varepsilon_i\right)\tau_i\left(T_{a,i} + T_{\text{sky}}\right), \tag{1a}$$

$$T_{B,j} = T_{a,j} + \tau_j \cdot \varepsilon_j \cdot T_s + \left(1-\varepsilon_j\right)\tau_j\left(T_{a,j} + T_{\text{sky}}\right), \tag{1b}$$

where $T_{B,i}$ and $T_{B,j}$ are the brightness temperatures at i and j GHz (Kelvins, hereafter referred as K); τ_i and τ_j are transmittances; $T_{a,i}$ and $T_{a,j}$ are the effective radiating temperatures of the atmosphere (K); ε_i and ε_j are LSEs; T_s is the land surface temperature (LST, K); and T_{sky} is the cosmic background radiation temperature (approximately 2.7 K). These equations implicitly include the dependence of the radiance on the sensor angle.

To reduce the number of parameters, we make two assumptions in this study. The first assumption is that $\varepsilon_i = \varepsilon_j$, which means that $\varepsilon \cdot T_s$ can be cancelled out when (1a) and (1b) are combined. This leads to a new combined equation without T_s:

$$\begin{aligned} &T_{B,i}\cdot\tau_j - T_{B,j}\cdot\tau_i + T_{a,j}\cdot\tau_i - T_{a,i}\cdot\tau_j \\ &\quad = (1-\varepsilon)\,\tau_i\cdot\tau_j\left(T_{a,i} - T_{a,j}\right). \end{aligned} \tag{2}$$

Several studies [54–56] have noted that a significant linear relationship exists between τ and PWV and between T_a and PWV. As a result, the terms $T_{a,j}\cdot\tau_i - T_{a,i}\cdot\tau_j$ and $\tau_i\cdot\tau_j(T_{a,i} - T_{a,j})$ in (2) can be expressed as quadratic and cubic equations about PWV. However, because it is more difficult to solve higher order equations than first order ones, the best forms about the two terms and PWV should be linear. Therefore, we make a second assumption that there are linear relationships between $T_{a,j}\cdot\tau_i - T_{a,i}\cdot\tau_j$ and PWV and between $\tau_i\cdot\tau_j(T_{a,i} - T_{a,j})$ and PWV. Under this assumption, (2) changes form as follows:

$$\begin{aligned} &T_{B,i}\cdot\left(\alpha_1\cdot\text{PWV} + \alpha_2\right) - T_{B,j}\cdot\left(\alpha_3\cdot\text{PWV} + \alpha_4\right) \\ &\quad + \left(\alpha_5\cdot\text{PWV} + \alpha_6\right) = (1-\varepsilon)\left(\alpha_7\cdot\text{PWV} + \alpha_8\right). \end{aligned} \tag{3}$$

The retrieval algorithm of PWV over land from passive microwave satellite data can be developed by simplifying (3) to the following form:

$$\mathrm{PWV} = \frac{\beta_1 + \beta_2 \cdot \varepsilon + \beta_3 \cdot T_{B,i} + \beta_4 \cdot T_{B,j}}{\beta_5 + \beta_6 \cdot \varepsilon + \beta_7 \cdot T_{B,i} + \beta_8 \cdot T_{B,j}}, \quad (4)$$

where β_i ($i = 1, \ldots, 8$) are coefficients, ε is the LSE, and $T_{B,i}$ and $T_{B,j}$ are brightness temperatures at i and j GHz (K). The retrieval algorithm is based on the two assumptions that (1) LSE at two adjacent frequencies are equal and (2) there are simple parameterizations that can relate transmittances, atmospheric effective radiating temperatures, and PWV. The two assumptions depend on the frequency and polarization of the brightness temperature data. Consequently, it is important to verify the accuracy of both assumptions by selecting the suitable combinations of frequency and polarization.

3.2. Verification of Assumptions. To retrieve PWV over land based on two types of brightness temperature data, both frequencies should possess two important qualities: significantly different atmospheric absorptions and approximately equal LSEs. The best way to ensure different atmospheric absorptions is to use one frequency in the vapor channel while the other is not. Thus, for the FY-3B MWRI, 23.8 GHz was selected because it is the only frequency in the water vapor channel. In addition to the 23.8 GHz band, two other bands at 18.7 and 36.5 GHz were considered as candidates because their LSE are approximately equal to the LSE for 23.8 GHz. To find the best solution, we further analyzed the LSE for 18.7, 23.8, and 36.5 GHz. Because the LSE is influenced by the rough surface and soil moisture content, the Advanced Integral Equation Model (AIEM) [57] was used to simulate LSE for different surfaces and soil moisture contents. AIEM can predict the backscattering and emissivity of Gaussian correlated surfaces, as demonstrated by comparisons of AIEM's results with experimental measurements [58, 59]. In this study, LSE were simulated at 18.7, 23.8, and 36.5 GHz, with an incidence angle of 53°, a correlation length of 15 cm, an RMS height of 1.0 cm (correlation length and RMS height are two fundamental physical quantities for describing the statistical characteristic of random rough surfaces), a soil temperature of 300 K, and a relative soil moisture content varying from 2% to 50% with a step of 2%. Using the simulated data, we calculated the variation in LSE at adjacent frequencies with increasing relative soil moisture content. The results are shown in Figure 1, and it is apparent that the maximum $\Delta\mathrm{LSE}_{23.8\text{-}18.7}$ is approximately 0.02; in contrast, the $\Delta\mathrm{LSE}_{36.5\text{-}23.8}$ is approximately 0.05, which indicates that the LSE at 18.7 GHz is much closer to the LSE at 23.8 GHz than to that at 36.5 GHz. As a consequence, 18.7 GHz was selected as the second frequency for the PWV retrieval model.

To further verify the first assumption that $\mathrm{LSE}_{18.7}$ is equal to $\mathrm{LSE}_{23.8}$, the polarization combination of the two frequencies was determined because different polarizations possess different LSE even at the same frequency. The LSE polarization differences at 18.7 and 23.8 GHz were compared to select the combination with a result closest to 0. The different LSE polarization combinations at 18.7 and 23.8 GHz are

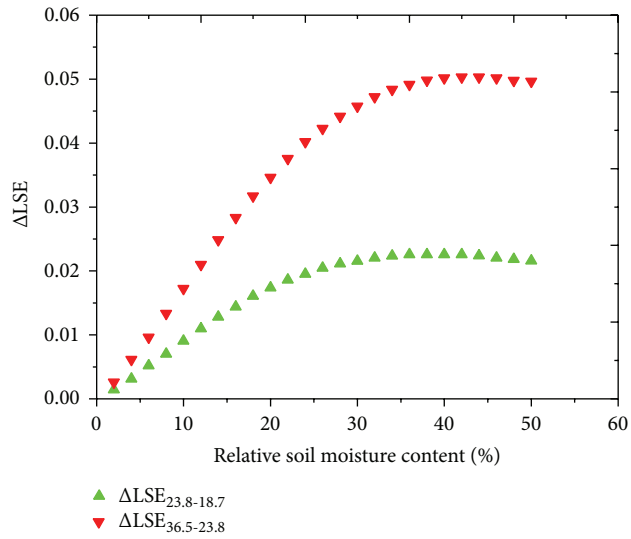

Figure 1: LSE differences at adjacent frequencies (18.7 and 23.8 GHz and 23.8 and 36.5 GHz) versus increasing relative soil moisture content.

expressed as $\Delta\mathrm{LSE}_{18.7\mathrm{v}\text{-}23.8\mathrm{v}}$, $\Delta\mathrm{LSE}_{18.7\mathrm{h}\text{-}23.8\mathrm{h}}$, $\Delta\mathrm{LSE}_{18.7\mathrm{v}\text{-}23.8\mathrm{h}}$, and $\Delta\mathrm{LSE}_{18.7\mathrm{h}\text{-}23.8\mathrm{v}}$ (v and h represent vertical and horizontal polarizations, resp.). Except for the previous simulation, this database also covers a wide range of surface dielectric constants, which are the averages calculated by the models of Dobson et al. [60], Mironov et al. [61], and Wang and Schmugge [62]. The corresponding volumetric soil moisture content varied from 2% to 50% with a step of 2%, the RMS height varied from 0.25 cm to 3.00 cm with a step of 0.25 cm, and the correlation length varied from 2.5 cm to 30 cm with a step of 2.5 cm. Figure 2 depicts the box charts of the four different LSE polarization combinations. The box chart of $\Delta\mathrm{LSE}_{18.7\mathrm{v}\text{-}23.8\mathrm{v}}$ is closest to the $y = 0$ line, followed by $\Delta\mathrm{LSE}_{18.7\mathrm{h}\text{-}23.8\mathrm{h}}$, $\Delta\mathrm{LSE}_{18.7\mathrm{v}\text{-}23.8\mathrm{h}}$, and $\Delta\mathrm{LSE}_{18.7\mathrm{h}\text{-}23.8\mathrm{v}}$. However, the simulated results showed no significant difference between $\Delta\mathrm{LSE}_{18.7\mathrm{h}\text{-}23.8\mathrm{h}}$ and $\Delta\mathrm{LSE}_{18.7\mathrm{v}\text{-}23.8\mathrm{v}}$. Moreover, $\Delta\mathrm{LSE}_{18.7\mathrm{h}\text{-}23.8\mathrm{h}}$ showed a minimum standard mean value of 0.0065, while the values for $\Delta\mathrm{LSE}_{18.7\mathrm{v}\text{-}23.8\mathrm{v}}$, $\Delta\mathrm{LSE}_{18.7\mathrm{v}\text{-}23.8\mathrm{h}}$, and $\Delta\mathrm{LSE}_{18.7\mathrm{h}\text{-}23.8\mathrm{v}}$ were 0.0069, 0.064, and 0.075, respectively. These results indicate that the differences in LSE for the same polarization at 18.7 and 23.8 GHz are less than for those for different polarizations, and the LSE differences for horizontal-horizontal polarizations are close to those for vertical-vertical polarizations. In addition, the box chart for $\Delta\mathrm{LSE}_{18.7\mathrm{h}\text{-}23.8\mathrm{h}}$ is the narrowest, indicating that the LSE for horizontal polarization is less sensitive to changes in soil dielectric constants than the LSE for vertical polarization. This insensitivity suggests that the horizontally polarized LSE is relatively stable even with large changes in land surface parameters. Given that it is important to maintain model robustness, the horizontal-horizontal polarization combination was selected for the PWV retrieval model.

The above analysis allowed us to select the best combination of frequencies and polarization (18.7 and 23.8 GHz with horizontal-horizontal polarization) for determination of

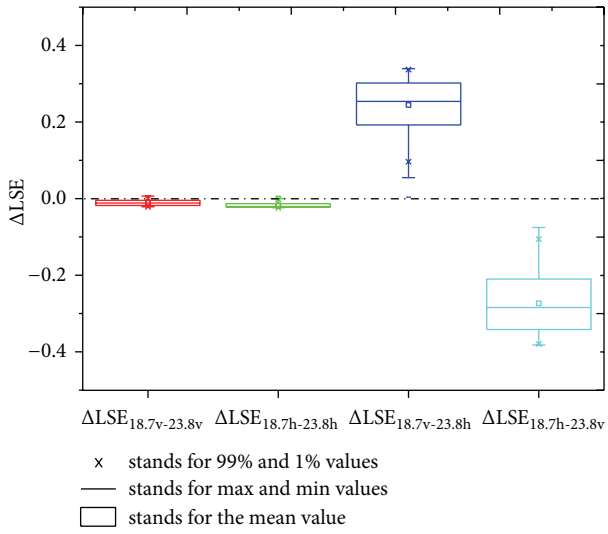

Figure 2: Box charts of four LSE polarization differences: $\Delta LSE_{18.7v\text{-}23.8v}$, $\Delta LSE_{18.7h\text{-}23.8h}$, $\Delta LSE_{18.7v\text{-}23.8h}$, and $\Delta LSE_{18.7h\text{-}23.8v}$.

PWV. Using these frequencies and polarization, we further investigate our second assumption.

To verify the relationships between the terms $T_{a,23.8} \cdot \tau_{18.7} - T_{a,18.7} \cdot \tau_{23.8}$ and PWV, as well as between $\tau_{18.7} \cdot \tau_{23.8}(T_{a,18.7} - T_{a,23.8})$ and PWV, a database including $T_{a,18.7}$, $T_{a,23.8}$, $\tau_{18.7}$, $\tau_{23.8}$, and PWV is necessary. In this study, MonoRTM was used to simulate these parameters along with TIGR profiles. MonoRTM is a radiative transfer model designed to process a number of monochromatic wavenumber values [63]. It is particularly useful in the microwave spectrum. The relationships between PWV and $T_{a,23.8} \cdot \tau_{18.7} - T_{a,18.7} \cdot \tau_{23.8}$ and between PWV and $\tau_{18.7} \cdot \tau_{23.8}(T_{a,18.7} - T_{a,23.8})$ are shown in Figure 3. As we expected, there is a significant linear relationship between $T_{a,23.8} \cdot \tau_{18.7} - T_{a,18.7} \cdot \tau_{23.8}$ and PWV with a coefficient of determination (R^2) of 0.99 and a Root Mean Square Error (RMSE) of 0.64 K. A linear relationship also exists between $\tau_{18.7} \cdot \tau_{23.8}(T_{a,18.7} - T_{a,23.8})$ and PWV with R^2 of 0.98 and an RMSE of 0.74 K. We note that Figure 3(b) displays more of a second order trend (with an R^2 of 0.99, not shown in the figure) than a linear trend. However, it is more difficult to solve a second order equation about PWV than a first order one; in addition, the trend of the second order equation is not much more significant than the trend of the first order one (R^2 of 0.99 versus R^2 of 0.98). Thus, we consider the first order equation for $\tau_{18.7} \cdot \tau_{23.8}(T_{a,18.7} - T_{a,23.8})$ and PWV to be acceptable, especially when PWV ranges from 5 to 40 mm. These results demonstrate that the second assumption is satisfied.

As stated previously, verification of the two assumptions provides a statistical basis for the PWV retrieval algorithm. Assuming that the lowest air temperature of each TIGR profile is the LST [64], and, using randomly generated numbers between 0.7 and 0.99 as the LSE, the brightness temperatures at 18.7 and 23.8 GHz were calculated with the forward models in (1a) and (1b), respectively. Afterwards, the coefficients (β_i; see Table 2) were calculated using the PWV, LSE, and brightness temperatures in (4) based on the nonlinear least squares optimization.

Table 2: Regression coefficients of the PWV retrieval algorithm applied only when using 18.7 and 23.8 GHz with horizontal polarization.

Coefficients	β_1	β_2	β_3	β_4	β_5	β_6	β_7	β_8
Values	−774.04	−211.41	−11.57	15.72	2.49	−19.15	0.2	−0.11

4. Results and Discussions

4.1. Sensitivity Analysis

4.1.1. Sensitivity of the PWV Retrieval Model to LSE Error. Our retrieval algorithm made the assumption that LSE was known through measurement or retrieval. However, either method can generate errors. To assess the sensitivity of the PWV retrieval model to LSE error, two series of normally distributed errors, $\text{error}_{\text{LSE}} \sim N(0, 0.01^2)$ and $\text{error}_{\text{LSE}} \sim N(0, 0.02^2)$ (the white noises whose mean is 0 and variances are 0.01 and 0.02, resp.), were added to the original LSE data. Using these new LSE data as input for the retrieval algorithm and leaving the other parameters unchanged, two new sets of estimated PWV were obtained with (4). Figure 4 shows the histograms of errors for the newly estimated PWV and the original PWV. It is apparent that there is an RMSE of 0.60 mm and a bias of 0.019 mm between the newly estimated PWV and the originally calculated values and that no LSE error exists. Moreover, over 99% of the errors are under 2 mm, which indicates that the PWV model is not very sensitive to errors in the LSE. Similarly, for LSE errors with a standard deviation of 0.02, there is an RMSE of 1.25 mm and a bias of 0.056 mm between the newly estimated and the original PWV values. This result further confirms that the error in LSE does not significantly affect the accuracy of PWV estimated using the proposed model.

4.1.2. Sensitivity of the PWV Retrieval Model to Brightness Temperature Error. In the retrieval model, $T_{B,18.7}$ and $T_{B,23.8}$ can be directly obtained from the brightness temperatures at 18.7 and 23.8 GHz with horizontal polarization. Consequently, errors are mainly introduced because of the noise-equivalent differential temperature (NEΔT) of the microwave radiometers, which are system errors. For FY-3B, the NEΔT values for brightness temperatures at 18.7 and 23.8 GHz are, respectively, 0.5 and 0.8 K. To assess the sensitivity of the PWV retrieval model to errors in T_B, two series of normally distributed errors, $\text{error}_{T_{B,18.7}} \sim N(0, 0.5^2)$ and $\text{error}_{T_{B,23.8}} \sim N(0, 0.8^2)$ (the white noises whose mean is 0 and variances are 0.5 and 0.8, resp.), were added to the original $T_{B,18.7}$ and $T_{B,23.8}$, respectively. These modified values were then used to obtain new estimates of PWV while leaving the other parameters unchanged. Figure 5 shows the histograms of errors between the newly estimated PWV and the original PWV. An RMSE of 1.23 mm and a bias of −0.014 mm result when the standard deviation of $T_{B,18.7}$ is 0.5 K. Moreover, over 90% of errors are less than

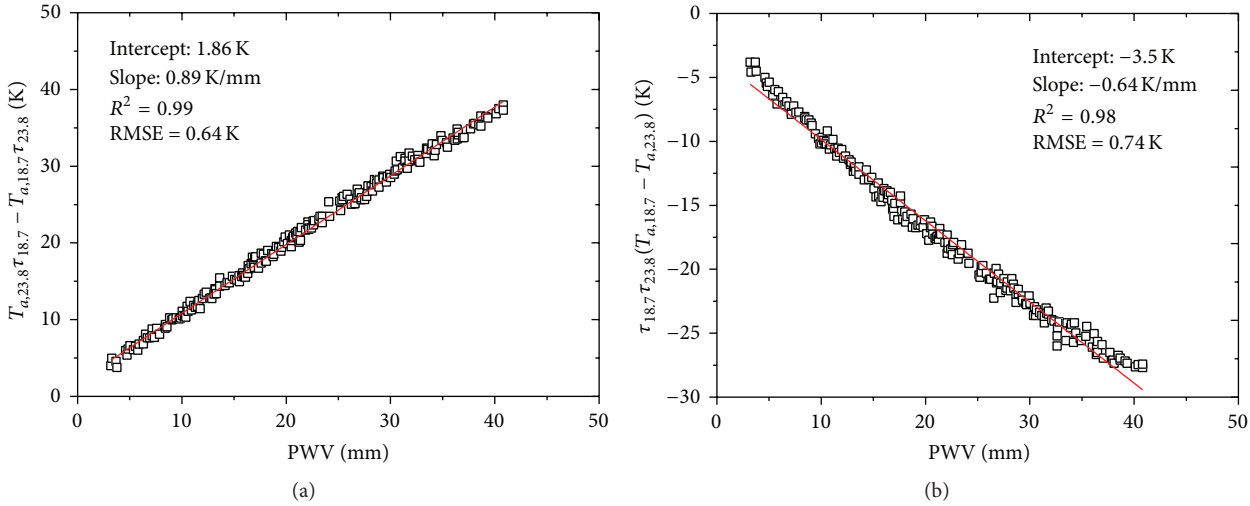

Figure 3: Linear relationships between (a) $T_{a,23.8} \cdot \tau_{18.7} - T_{a,18.7} \cdot \tau_{23.8}$ and PWV and (b) $\tau_{18.7} \cdot \tau_{23.8}(T_{a,18.7} - T_{a,23.8})$ and PWV.

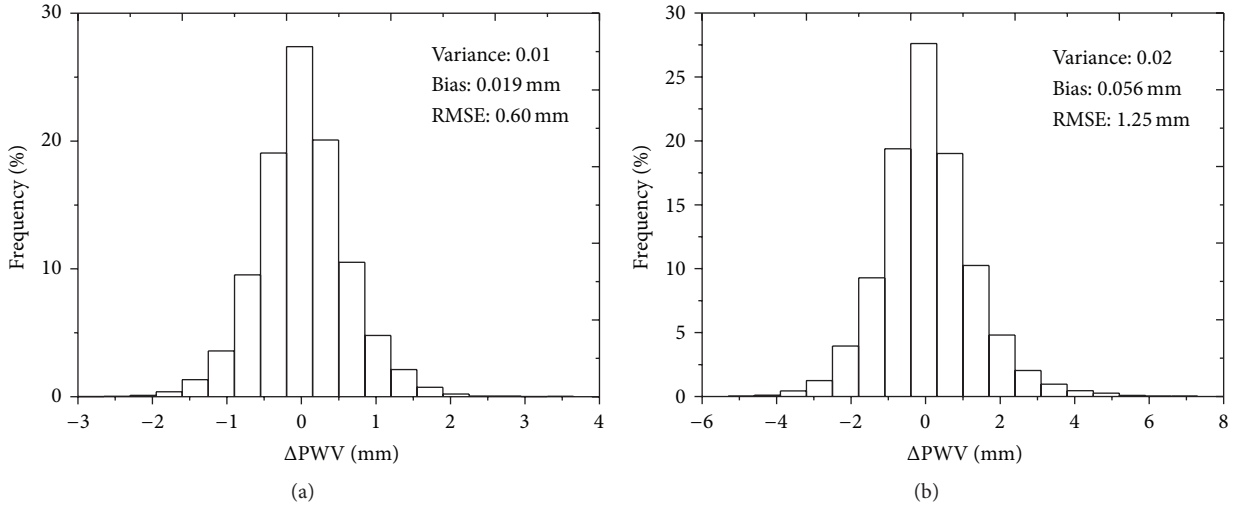

Figure 4: Histograms of errors between the newly estimated PWV (using the new LSE, which includes added errors) and the original PWV when (a) the standard deviation of the LSE errors is 0.01 and (b) the standard deviation of the LSE errors is 0.02.

2 mm and less than 0.3% of errors are over 4 mm, which indicates that the PWV model is not sensitive to error in $T_{B,18.7}$. On the contrary, a $T_{B,23.8}$ error with a standard deviation of 0.8 K results in an RMSE of 2.05 mm, which is greater than the RMSE for LSE and $T_{B,18.7}$. In addition, approximately 67% of errors are less than 2 mm and approximately 5% of errors are greater than 4 mm. Thus, the PWV algorithm is more sensitive to errors in $T_{B,23.8}$ than to errors in LSE and $T_{B,18.7}$. In realistic case, the errors normally occur simultaneously in both channels; thus, we discuss the sensitivity of the PWV retrieval model to both channels errors (0.5 K for $T_{B,18.7}$ and 0.8 K for $T_{B,23.8}$, not shown). An RMSE of 2.43 mm and a bias of 0.0064 mm are obtained with 61% of errors less than 2 mm and approximately 9% of errors greater than 4 mm. It is found that the RMSE caused by both channels errors is not the sum of two separate RMSE caused by both $T_{B,23.8}$ and $T_{B,23.8}$ errors. This is because the different error sources are counteracted in practice. Fortunately, however, because the source of $T_{B,23.8}$ errors is NEΔT, these errors can be dealt with by promoting better design and manufacture of microwave radiometers. These improvements could further reduce the sensitivity of the PWV retrieval model to errors in $T_{B,23.8}$ in the future.

4.2. Validation. To further assess the accuracy of the PWV retrieval model, validations were performed using L band radiosonde sounding observations and AERONET CE318-PWV products, respectively. FY-3B MWRI brightness temperatures at 18.7 and 23.8 GHz with horizontal polarization were extracted and used as input data of the algorithm. Because a radiosonde's investigation radius can be up to 200 km (depending on the wind speed and direction at various altitudes), the radiosonde sounding observations can

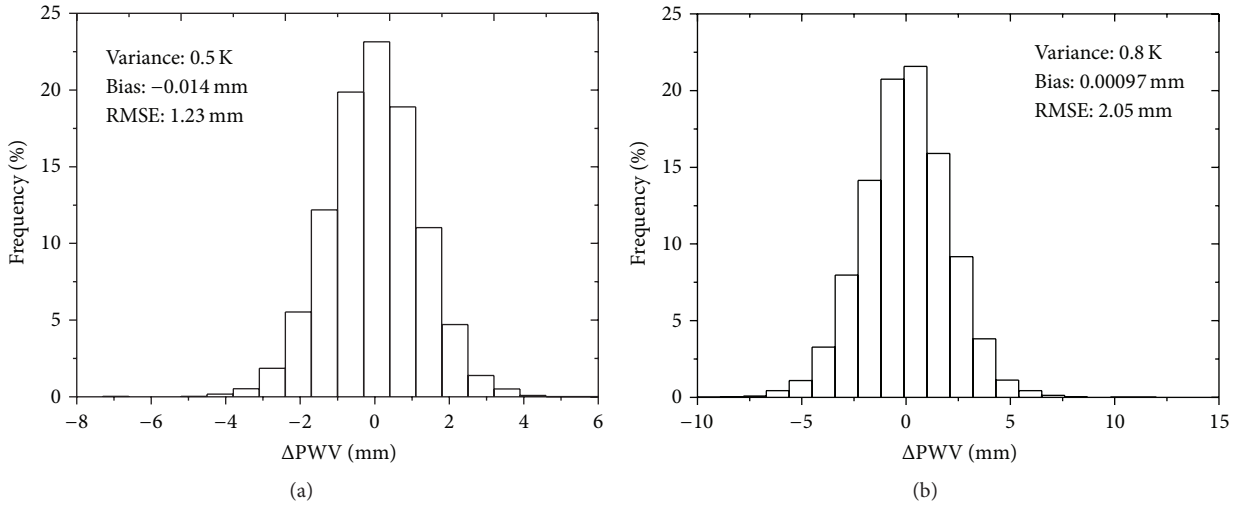

FIGURE 5: Histograms of errors between the newly estimated PWV (using the new brightness temperatures with added errors) and the original PWV when (a) the standard deviation of the $T_{B,18.7}$ errors is 0.5 K and (b) the standard deviation of the $T_{B,23.8}$ errors is 0.8 K.

represent the atmospheric conditions of an entire MWRI pixel. Considering the orbital gaps in the FY-3B MWRI data, only 58 available data were selected, including 34 cloudy days and 24 cloud-free days. Because no available daily or hourly LSE products exist, the instantaneous LSE values used in the validation were calculated using the following equation (adapted from (1a) and (1b)):

$$\mathrm{LSE} = \frac{T_{B,18.7} - T_{a,18.7} - \tau_{18.7}\left(T_{a,18.7} + T_{\mathrm{sky}}\right)}{\tau_{18.7} \cdot T_s' - \tau_{18.7}\left(T_{a,18.7} + T_{\mathrm{sky}}\right)}, \quad (5)$$

where $T_{B,18.7}$ is the brightness temperature at 18.7 GHz (K), $\tau_{18.7}$ is the transmittance, $T_{a,18.7}$ is the effective radiating temperature of the atmosphere (K), T_s' is the LST (because no infrared LST products exist for cloudy days, measured LST values from Zhangye National Climate Observatory were used) (K), and T_{sky} is the cosmic background radiation temperature (2.7 K).

Figure 6 shows comparisons of the corrected radiosonde PWV and the retrieved PWV for both cloudy and cloud-free days. On cloud-free days, the retrieval algorithm overestimates the PWV with an RMSE of 4.39 mm and a bias of 0.36 mm compared to the radiosonde PWV. These errors mainly derive from three sources. First, the model itself error still exists. Second, the detection zone of radiosonde balloons ranges from the land surface to an altitude of approximately 30–35 km; in contrast, the FY-3B satellite orbits the earth at an altitude of 836 km. This difference in detection zones causes the retrieved PWV from FY-3B to theoretically be more than the radiosonde PWV. This explains the positive bias in the comparison. Third, there are errors from the measured $T_{B,18.7}$ and $T_{B,23.8}$ and the retrieved LSE, and, analyzed hereinbefore, the effects of these errors are small except $T_{B,23.8}$. On cloudy days, the retrieval algorithm overestimates the PWV with an RMSE of 4.84 mm and a bias of 0.52 mm. The additional errors on cloudy days are mainly caused by liquid water and water ice in clouds, which affect the transmittance,

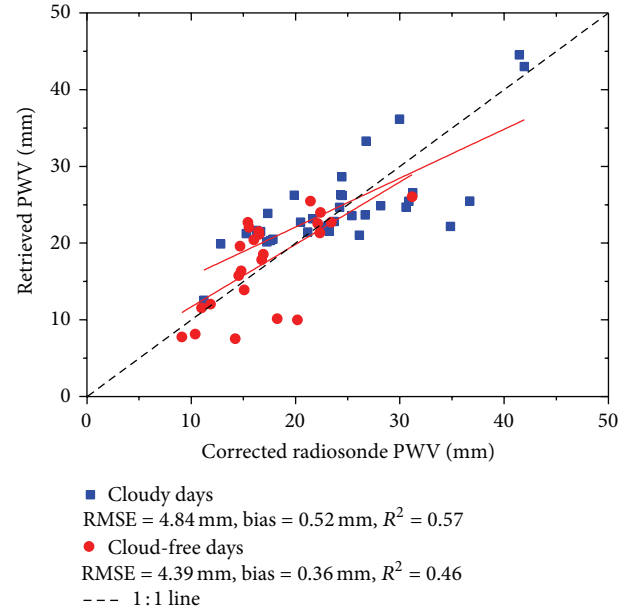

FIGURE 6: Comparison of the corrected radiosonde PWV and retrieved PWV for cloud-free days (red circles) and cloudy days (blue squares) at Zhangye National Climate Observatory.

atmospheric effective radiating temperature, and brightness temperature because of volume scattering and absorption of water. Figure 7 compares the corrected AERONET PWV at Dalanzadgad (in dry area) and Singapore (in tropical region) and the retrieved PWV on cloud-free conditions. On the whole, the retrieval algorithm shows a satisfactory accuracy for the dry area and tropical region with a total RMSE of 4.73 mm and a bias of 0.84 mm. But it is noted that the retrieval algorithm reveals an overestimation when PWV is lower than 10 mm and an underestimation when PWV is higher than 40 mm. This may be because we consider the first

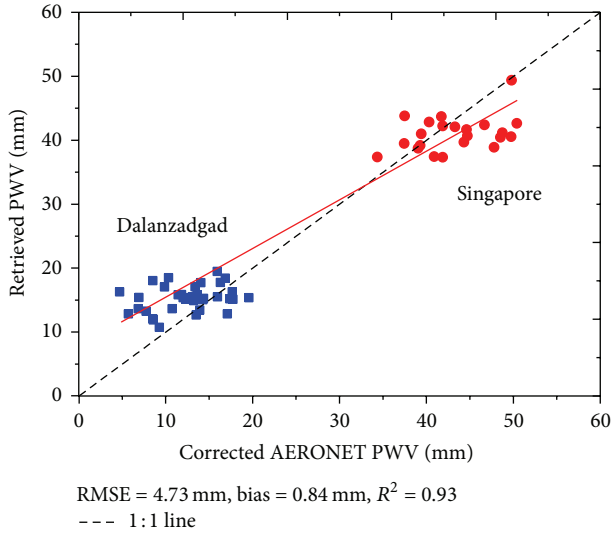

FIGURE 7: Comparison of the corrected AERONET PWV and the retrieved PWV for cloud-free conditions at Dalanzadgad (in dry area) and Singapore (in tropical region) sites.

order equation for $\tau_{18.7} \cdot \tau_{23.8}(T_{a,18.7} - T_{a,23.8})$ and PWV rather than second order, leading to the errors when the water vapor is very dry or very moist.

4.3. Discussions. As the input parameters of the model, LSE is very important because it often has greater error compared to the brightness temperatures as the high-level remotely sensed product. But sensitivity analysis reveals that this algorithm is insensitive to the LSE error. Besides, this algorithm does not need LST as the input data, which further reduces the potential error from LST product. Both suggest that this algorithm has better robustness compared to previous researches [43, 44]. On cloudy days, although the accuracy is inferior to that of cloud-free days, this retrieval algorithm shows the ability to provide the PWV distribution, at which time no infrared PWV products are available [65]. The effects of water scattering and absorption in clouds are ignored in our retrieval algorithm because of their complexity, while one thing which fascinates us is that from Figure 6 we can find that RMSE and bias on cloudy days are only a little higher than those on cloud-free days; the performances of RMSE and bias are far from the expectation that the accuracy degrades significantly on cloudy days. This may be caused by two reasons: first, the cloud liquid water is little on these cloudy days and the PWV retrieval algorithm is insensitive to it; second, the validation data are sparse and under representation. To further improve the algorithm's accuracy, we will consider the water scattering and absorption for microwave radiation in future studies.

5. Conclusions

An algorithm for retrieving PWV over land was developed based on passive microwave brightness temperature data at 18.7 and 23.8 GHz with horizontal polarization. The algorithm is based on two assumptions: first, that LSE is equal at two adjacent frequencies and, second, that simple parameterizations exist which relate transmittance, atmospheric effective radiating temperature, and PWV. Using simulated data from two widely used and physically based models, AIEM and MonoRTM, we confirmed these two assumptions. To assess the precision of the retrieval model, L band radiosonde sounding observations and AERONET sun photometers were collected and were used to verify the retrieved PWV. Our results revealed a significant relationship between the retrieved PWV and the corrected radiosonde and AERONET PWV products both on cloud-free and on cloudy days and both in dry area and in tropical region.

It is difficult to completely distinguish the atmospheric signal from the surface background. The advance in this retrieval model lies in the reduction in input parameters. Without LST observations, this PWV retrieval model is much easier and reduces the potential errors from the LST products. Meanwhile, this model possesses some physical foundation because it is developed from the radiative transfer equation. Validation suggests that the algorithm performs well on cloud-free days but worse on cloudy days due to the volume scattering and absorption of water, which is ignored in this model. To generalize the model, the effects of cloud liquid water on the PWV retrieval algorithm should be considered in future work. The accuracy of the model could also be further assessed using additional PWV data.

Conflict of Interests

The authors declare that there is no conflict of interests regarding the publication of this paper.

Acknowledgments

This work was supported by the National Natural Science Foundation of China under Grant no. 41231170 and an independent innovation project of State Key Laboratory of Resource and Environmental Information System, CAS (no. 08R8B6B0YA). The authors thank the ARA for providing the TIGR dataset, the AER for providing the MonoRTM code, and WestDC (http://westdc.westgis.ac.cn/) for providing the dataset of radiosonde sounding observations from Zhangye National Climate Observatory.

References

[1] M. Bevis, S. Businger, T. A. Herring, C. Rocken, R. A. Anthes, and R. H. Ware, "GPS meteorology: remote sensing of atmospheric water vapor using the global positioning system," *Journal of Geophysical Research*, vol. 97, no. 14, pp. 15787–15801, 1992.

[2] I. M. Held and B. J. Soden, "Water vapor feedback and global warming," in *Annual Review of Energy and the Environment*, pp. 441–475, Annual Reviews Inc, Palo Alto, Calif, USA, 2000.

[3] C. O. Justice, T. F. Eck, D. Tanre, and B. N. Holben, "The effect of water-vapor on the normalized difference vegetation index derived for the sahelian region from NOAA AVHRR data,"

International Journal of Remote Sensing, vol. 12, no. 6, pp. 1165–1187, 1991.

[4] J. A. Sobrino, Z.-L. Li, and M. P. Stoll, "Impact of the atmospheric transmittance and total water vapor content in the algorithms for estimating satellite sea surface temperatures," *IEEE Transactions on Geoscience and Remote Sensing*, vol. 31, no. 5, pp. 946–952, 1993.

[5] J. A. Sobrino, Z.-L. Li, M. P. Stoll, and F. Becker, "Improvements in the split-window technique for land surface temperature determination," *IEEE Transactions on Geoscience and Remote Sensing*, vol. 32, no. 2, pp. 243–253, 1994.

[6] B.-H. Tang, Y. Y. Bi, Z.-A. Li, and J. Xia, "Generalized split-window algorithm for estimate of land surface temperature from Chinese geostationary FengYun meteorological satellite (FY-2C) data," *Sensors*, vol. 8, no. 2, pp. 933–951, 2008.

[7] J.-P. Chaboureau, A. Chédin, and N. A. Scott, "Remote sensing of the vertical distribution of atmospheric water vapor from the TOVS observations: method and validation," *Journal of Geophysical Research: Atmospheres*, vol. 103, no. 8, pp. 8743–8752, 1998.

[8] H. Wu, L. Ni, N. Wang, Y. Qian, B.-H. Tang, and Z.-L. Li, "Estimation of atmospheric profiles from hyperspectral infrared IASI sensor," *IEEE Journal of Selected Topics in Applied Earth Observations and Remote Sensing*, vol. 6, no. 3, pp. 1485–1494, 2013.

[9] Z.-L. Li, L. Jia, Z. B. Su, Z. M. Wan, and R. H. Zhang, "A new approach for retrieving precipitable water from ATSR2 split-window channel data over land area," *International Journal of Remote Sensing*, vol. 24, no. 24, pp. 5095–5117, 2003.

[10] S. Peng, B.-H. Tang, H. Wu, R. Tang, and Z.-L. Li, "Estimating of the total atmospheric precipitable water vapor amount from the Chinese new generation polar orbit FengYun meteorological satellite (FY-3) data," in *Proceedings of the IEEE International Geoscience and Remote Sensing Symposium (IGARSS '14)*, pp. 3029–3032, IEEE, Québec, Canada, July 2014.

[11] A. E. Niell, A. J. Coster, F. S. Solheim et al., "Comparison of measurements of atmospheric wet delay by radiosonde, water vapor radiometer, GPS, and VLBI," *Journal of Atmospheric and Oceanic Technology*, vol. 18, no. 6, pp. 830–850, 2001.

[12] D. Pérez-Ramírez, D. N. Whiteman, A. Smirnov et al., "Evaluation of AERONET precipitable water vapor versus microwave radiometry, GPS, and radiosondes at ARM sites," *Journal of Geophysical Research: Atmospheres*, vol. 119, no. 15, pp. 9596–9613, 2014.

[13] R. N. Halthore, T. F. Eck, B. N. Holben, and B. L. Markham, "Sun photometric measurements of atmospheric water vapor column abundance in the 940-nm band," *Journal of Geophysical Research: Atmospheres*, vol. 102, no. 4, pp. 4343–4352, 1997.

[14] B. N. Holben and T. F. Eck, "Precipitable water in the Sahel measured using sun photometry," *Agricultural and Forest Meteorology*, vol. 52, no. 1-2, pp. 95–107, 1990.

[15] J. J. Michalsky, J. C. Liljegren, and L. C. Harrison, "A comparison of Sun photometer derivations of total column water vapor and ozone to standard measures of same at the Southern Great Plains Atmospheric Radiation Measurement site," *Journal of Geophysical Research Atmospheres*, vol. 100, no. 12, pp. 25995–26003, 1995.

[16] F. E. Volz, "Economical multispectral sun photometer for measurements of aerosol extinction from 0.44 μm to 1.6 μm and precipitable water," *Applied Optics*, vol. 13, no. 8, pp. 1732–1733, 1974.

[17] D. A. Leonard, "Observation of raman scattering from the atmosphere using a pulsed nitrogen ultraviolet laser," *Nature*, vol. 216, no. 5111, pp. 142–143, 1967.

[18] J. A. Cooney, "Measurements on the raman component of laser atmospheric backscatter," *Applied Physics Letters*, vol. 12, no. 2, pp. 40–42, 1968.

[19] W. B. Grant, "Differential absorption and Raman lidar for water vapor profile measurements: a review," *Optical Engineering*, vol. 30, no. 1, pp. 40–48, 1991.

[20] M. Froidevaux, C. W. Higgins, V. Simeonov et al., "A Raman lidar to measure water vapor in the atmospheric boundary layer," *Advances in Water Resources*, vol. 51, pp. 345–356, 2013.

[21] D. N. Whiteman, K. Rush, S. Rabenhorst et al., "Airborne and ground-based measurements using a high-performance raman lidar," *Journal of Atmospheric and Oceanic Technology*, vol. 27, no. 11, pp. 1781–1801, 2010.

[22] D. C. Hogg, F. O. Guiraud, J. B. Snider, M. T. Decker, and E. R. Westwater, "A steerable dual-channel microwave radiometer for measurement of water vapor and liquid in the troposphere," *Journal of Applied Meteorology*, vol. 22, no. 5, pp. 789–806, 1983.

[23] F. O. Guiraud, J. Howard, and D. C. Hogg, "A dual-channel microwave radiometer for measurement of precipitable water vapor and liquid," *IEEE Transactions on Geoscience Electronics*, vol. 17, no. 4, pp. 129–136, 1979.

[24] D. Cimini, T. J. Hewison, and L. Martin, "Comparison of brightness temperatures observed from ground-based microwave radiometers during TUC," *Meteorologische Zeitschrift*, vol. 15, no. 1, pp. 19–25, 2006.

[25] M. P. Cadeddu, J. C. Liljegren, and D. D. Turner, "The atmospheric radiation measurement (ARM) program network of microwave radiometers: instrumentation, data, and retrievals," *Atmospheric Measurement Techniques*, vol. 6, no. 9, pp. 2359–2372, 2013.

[26] T. R. Emardson, J. Johansson, and G. Elgered, "The systematic behavior of water vapor estimates using four years of GPS observations," *IEEE Transactions on Geoscience and Remote Sensing*, vol. 38, no. 1, pp. 324–329, 2000.

[27] Y. A. Liou, Y. T. Teng, T. V. Hove, and J. C. Liljegren, "Comparison of precipitable water observations in the near tropics by GPS, microwave radiometer, and radiosondes," *Journal of Applied Meteorology*, vol. 40, no. 1, pp. 5–15, 2001.

[28] J. Chen and G. Li, "Diurnal variations of ground-based GPS-PWV under different solar radiation intensity in the Chengdu Plain," *Journal of Geodynamics*, vol. 72, pp. 81–85, 2013.

[29] B.-C. Gao and Y. J. Kaufman, "Water vapor retrievals using Moderate Resolution Imaging Spectroradiometer (MODIS) near-infrared channels," *Journal of Geophysical Research D: Atmospheres*, vol. 108, no. 13, pp. 1–10, 2003.

[30] Z. Li, J.-P. Muller, and P. Cross, "Comparison of precipitable water vapor derived from radiosonde, GPS, and moderate-resolution imaging spectroradiometer measurements," *Journal of Geophysical Research: Atmospheres*, vol. 108, no. 20, pp. 10-1–10-12, 2003.

[31] D. C. Tobin, H. E. Revercomb, R. O. Knuteson et al., "Atmospheric radiation measurement site atmospheric state best estimates for atmospheric infrared sounder temperature and water vapor retrieval validation," *Journal of Geophysical Research D: Atmospheres*, vol. 111, no. 9, pp. 831–846, 2006.

[32] H. H. Aumann, M. T. Chahine, C. Gautier et al., "AIRS/AMSU/HSB on the aqua mission: design, science objectives, data products, and processing systems," *IEEE*

Transactions on Geoscience and Remote Sensing, vol. 41, no. 2, pp. 253–264, 2003.

[33] J. Susskind, C. D. Barnet, and J. M. Blaisdell, "Retrieval of atmospheric and surface parameters from AIRS/AMSU/HSB data in the presence of clouds," *IEEE Transactions on Geoscience and Remote Sensing*, vol. 41, no. 2, pp. 390–409, 2003.

[34] P. Schluessel and W. J. Emery, "Atmospheric water vapour over oceans from SSM/I measurements," *International Journal of Remote Sensing*, vol. 11, no. 5, pp. 753–766, 1990.

[35] F. Wentz and T. Meissner, "AMSR ocean algorithm, version 2, algorithm theoretical basis document," Tech. Rep. 121599A-1, Remote Sensing System, Santa Rosa, Calif, USA, 2000.

[36] P. Basili, S. Bonafoni, V. Mattioli, P. Ciotti, and N. Pierdicca, "Mapping the atmospheric water vapor by integrating microwave radiometer and GPS measurements," *IEEE Transactions on Geoscience and Remote Sensing*, vol. 42, no. 8, pp. 1657–1665, 2004.

[37] S.-A. Boukabara, K. Garrett, and C. Wanchun, "Global coverage of total precipitable water using a microwave variational algorithm," *IEEE Transactions on Geoscience and Remote Sensing*, vol. 48, no. 10, pp. 3608–3621, 2010.

[38] F. Aires, C. Prigent, W. B. Rossow, and M. Rothstein, "A new neural network approach including first guess for retrieval of atmospheric water vapor, cloud liquid water path, surface temperature, and emissivities over land from satellite microwave observations," *Journal of Geophysical Research: Atmospheres*, vol. 106, no. 14, pp. 14887–14907, 2001.

[39] P. Basili, S. Bonafoni, V. Mattioli et al., "Neural-network retrieval of integrated precipitable water vapor over land from satellite microwave radiometer," in *Proceedings of the 11th Specialist Meeting on Microwave Radiometry and Remote Sensing of the Environment (MicroRad '10)*, pp. 161–166, IEEE, Washington, DC, USA, March 2010.

[40] S. Bonafoni, V. Mattioli, P. Basili, P. Ciotti, and N. Pierdicca, "Satellite-based retrieval of precipitable water vapor over land by using a neural network approach," *IEEE Transactions on Geoscience and Remote Sensing*, vol. 49, no. 9, pp. 3236–3248, 2011.

[41] J. Miao, K. Kunzi, G. Heygster, T. A. Lachlan-Cope, and J. Turner, "Atmospheric water vapor over Antarctica derived from Special Sensor Microwave/Temperature 2 data," *Journal of Geophysical Research: Atmospheres*, vol. 106, no. 10, pp. 10187–10203, 2001.

[42] K.-P. Johnsen, J. Miao, and S. Q. Kidder, "Comparison of atmospheric water vapor over Antarctica derived from CHAMP/GPS and AMSU-B data," *Physics and Chemistry of the Earth, Parts A/B/C*, vol. 29, no. 2-3, pp. 251–255, 2004.

[43] M. N. Deeter, "A new satellite retrieval method for precipitable water vapor over land and ocean," *Geophysical Research Letters*, vol. 34, no. 2, Article ID L02815, 2007.

[44] D. Ji and J. Shi, "Water vapor retrieval over cloud cover area on land using AMSR-E and MODIS," *IEEE Journal of Selected Topics in Applied Earth Observations and Remote Sensing*, vol. 7, no. 7, pp. 3105–3116, 2014.

[45] H. Yang, X. Zou, X. Li, and R. You, "Environmental data records from FengYun-3B microwave radiation imager," *IEEE Transactions on Geoscience and Remote Sensing*, vol. 50, no. 12, pp. 4986–4993, 2012.

[46] Thermodynamic Initial Guess Retrieval (TIGR), August 2015, http://ara.abct.lmd.polytechnique.fr/index.php?page=tigr.

[47] FENGYUN Satellite Data Center, August 2015, http://satellite.cma.gov.cn/PortalSite/Default.aspx.

[48] J. C. Bian, H. B. Chen, H. Vömel, Y. J. Duan, Y. J. Xuan, and D. R. Lü, "Intercomparison of humidity and temperature sensors: GTS1, Vaisala RS80, and CFH," *Advances in Atmospheric Sciences*, vol. 28, no. 1, pp. 139–146, 2011.

[49] L. M. Miloshevich, H. Vömel, D. N. Whiteman, and T. Leblanc, "Accuracy assessment and correction of Vaisala RS92 radiosonde water vapor measurements," *Journal of Geophysical Research Atmospheres*, vol. 114, no. 11, pp. 1013–1033, 2009.

[50] B. N. Holben, T. F. Eck, I. Slutsker et al., "AERONET—a federated instrument network and data archive for aerosol characterization," *Remote Sensing of Environment*, vol. 66, no. 1, pp. 1–16, 1998.

[51] A. Smirnov, B. N. Holben, T. F. Eck, O. Dubovik, and I. Slutsker, "Cloud-screening and quality control algorithms for the AERONET database," *Remote Sensing of Environment*, vol. 73, no. 3, pp. 337–349, 2000.

[52] O. Dubovik, A. Smirnov, B. N. Holben et al., "Accuracy assessments of aerosol optical properties retrieved from Aerosol Robotic Network (AERONET) sun and sky radiance measurements," *Journal of Geophysical Research: Atmospheres*, vol. 105, no. 8, pp. 9791–9806, 2000.

[53] Z.-L. Li, B.-H. Tang, H. Wu et al., "Satellite-derived land surface temperature: current status and perspectives," *Remote Sensing of Environment*, vol. 131, pp. 14–37, 2013.

[54] Z.-L. Liu, H. Wu, B.-H. Tang, S. Qiu, and Z.-L. Li, "Atmospheric corrections of passive microwave data for estimating land surface temperature," *Optics Express*, vol. 21, no. 13, pp. 15654–15663, 2013.

[55] Z.-L. Liu, H. Wu, B.-H. Tang, S. Qiu, and Z.-L. Li, "An empirical relationship of bare soil microwave emissions between vertical and horizontal polarization at 10.65 GHz," *IEEE Geoscience and Remote Sensing Letters*, vol. 11, no. 9, pp. 1479–1483, 2014.

[56] E. R. Westwater, J. B. Snider, and M. J. Falls, "Ground-based radiometric observations of atmospheric emission and attenuation at 20.6, 31.65, and 90.0 GHz: a comparison of measurements and theory," *IEEE Transactions on Antennas and Propagation*, vol. 38, no. 10, pp. 1569–1580, 1990.

[57] K. S. Chen, T.-D. Wu, L. Tsang, Q. Li, J. Shi, and A. K. Fung, "Emission of rough surfaces calculated by the integral equation method with comparison to three-dimensional moment method simulations," *IEEE Transactions on Geoscience and Remote Sensing*, vol. 41, no. 1, pp. 90–101, 2003.

[58] J. C. Shi, L. M. Jiang, L. X. Zhang, K.-S. Chen, J.-P. Wigneron, and A. Chanzy, "A parameterized multifrequency-polarization surface emission model," *IEEE Transactions on Geoscience and Remote Sensing*, vol. 43, no. 12, pp. 2831–2841, 2005.

[59] L. Chen, J. Shi, J.-P. Wigneron, and K.-S. Chen, "A parameterized surface emission model at L-band for soil moisture retrieval," *IEEE Geoscience and Remote Sensing Letters*, vol. 7, no. 1, pp. 127–130, 2010.

[60] M. C. Dobson, F. T. Ulaby, M. T. Hallikainen, and M. A. El-Rayes, "Microwave dielectric behavior of wet soil—part II: dielectric mixing models," *IEEE Transactions on Geoscience and Remote Sensing*, vol. 23, no. 1, pp. 35–46, 1985.

[61] V. L. Mironov, M. C. Dobson, V. H. Kaupp, S. A. Komarov, and V. N. Kleshchenko, "Generalized refractive mixing dielectric model for moist soils," *IEEE Transactions on Geoscience and Remote Sensing*, vol. 42, no. 4, pp. 773–785, 2004.

[62] J. R. Wang and T. J. Schmugge, "An empirical model for the complex dielectric permittivity of soils as a function of water content," *IEEE Transactions on Geoscience and Remote Sensing*, vol. 18, no. 4, pp. 288–295, 1980.

[63] MonoRTM, August 2015, http://rtweb.aer.com/monortm_frame.html.

[64] M. J. McFarland, R. L. Miller, and C. M. U. Neale, "Land surface temperature derived from the SSM/I passive microwave brightness temperatures," *IEEE Transactions on Geoscience and Remote Sensing*, vol. 28, no. 5, pp. 839–845, 1990.

[65] Y. J. Kaufman and B.-C. Gao, "Remote sensing of water vapor in the near IR from EOS/MODIS," *IEEE Transactions on Geoscience and Remote Sensing*, vol. 30, no. 5, pp. 871–884, 1992.